Insights into the atomic and electronic structure triggered by ordered nitrogen vacancies in CrN

Zaoli Zhang,[1] Hong Li,[1] Rostislav Daniel,[2] Christian Mitterer,[2] and Gerhard Dehm[1,3]
[1]*Erich Schmid Institute of Materials Science, Austrian Academy of Sciences, Leoben, Austria*
[2]*Department of Physical Metallurgy and Materials Testing, Montanuniversität Leoben, Austria*
[3]*Department of Materials Physics, Montanuniversität Leoben, Leoben, Austria*
(Received 29 July 2012; revised manuscript received 21 November 2012; published 8 January 2013)

We report on the atomic and electronic structure of ordered nitrogen vacancies in CrN by using spherical aberration-corrected high-resolution transmission electron microscopy, electron energy-loss spectra, and *ab initio* calculations. The ordered nitrogen vacancies are identified to be distributed on {111} atomic planes. The vacancy concentrations were evaluated by quantitative high-resolution transmission electron microscopy. A direct consequence of the ordered nitrogen vacancies is a lattice shrinking leading to a reduced lattice constant, displaying a distorted CrN. The experimental measured lattice constant is quantitatively compared to the *ab initio* calculations. A relationship between the lattice constant and nitrogen vacancy concentration is theoretically and experimentally established, and quantitatively compared. The presence of the ordered N vacancies further induces the electronic changes as reflected in a very small core-level shift as well as a shift of the volume plasmon energy. Moreover, the change of the ionicity in CrN with nitrogen vacancy concentration is revealed. A direct relation between the covalent-ionic level of the bonding and the nitrogen vacancy concentration is shown.

DOI: 10.1103/PhysRevB.87.014104 PACS number(s): 61.72.jd, 61.05.−a, 68.37.Og, 79.20.Uv

I. INTRODUCTION

Transition metal nitrides are known as hard metallic compounds that are characterized by their extreme hardness, thermal stability, and resistance to corrosion. As a consequence, they have found numerous applications in the cutting- and machining-tool industry.[1] Typical materials are TiN, TiAlN, and CrN.[1–3] Among them, CrN has—besides its application as wear-resistant coating—recently gained considerable interest[4–13] as it has unique antiferromagnetic configurations, and has been used as a prototype material for strong magnetrostructural interactions.[4] CrN has an orthorhombic crystal structure and antiferromagnetic properties below a Néel temperature (T_N) of ∼286 K, and transforms into a cubic paramagnetic insulator above the T_N. The studies relevant to CrN films can be simply classified into structural studies[2–4,6,13] and electrical, optical, and mechanical property measurements.[5,8,10] Furthermore, structural calculations using density functional theory (DFT)[7] have also been performed. However, controversial results were obtained regarding whether CrN possess a metallic or semiconductor electronic structure.[5,8,10,14,15] The discrepancy is essentially closely related to the different crystalline quality of the samples, such as various defects, which were used by different authors. The defects and their critical densities in the film can alter the electronic structure of CrN.[11] The frequently encountered defects are nitrogen (N) vacancies, which are known to act as carriers, that is, donors, and play an important role for the resulting electronic properties of CrN.[11]

It is noted that the stoichiometry or structural defects, such as vacancies, interstitial atoms, and dislocations, influence the properties of transition metal nitrides.[1,16,17] The knowledge about the influence of N vacancies on phase stability and mechanical properties of CrN coatings is still in its infancy. Thus, systematic data based on a comprehensive characterization of N vacancy effects in CrN is definitely needed. It was reported that these N vacancies can affect the chemical bonding and electronic structures as revealed by x-ray photoemission spectroscopy in TiVN and TiN_x,[16,18,19] by electron energy-loss spectroscopy (EELS) in TiN_x,[20,21] and VN_x.[22,23] Theoretical calculations uncover that N vacancies can strongly affect the mechanical properties[17] and thermally induce atomic changes in TiN.[24]

So far, experimentally evaluating the atomic and electronic structure changes induced by N vacancies in hard coating materials is relatively scarce, although it is obviously of importance for understanding the various properties of transition metal nitrides. It seems conceivable that the study of simultaneous atomic and electronic structures enabled by a combination of modern spherical aberration-corrected (C_S-corrected) high-resolution transmission electron microscopy (HRTEM), scanning transmission electron microscopy (STEM), and EELS, can elucidate the effects caused by N vacancies. It is known that a substoichiometric CrN could occur during CrN synthesis, and N vacancies and other defects are consequently likely to be introduced. Despite this fact, however, characterizing the atomic and electronic structures of N vacancies at the atomic scale is still not yet available. Particularly for CrN, a fundamental knowledge is required to advance the performance of this material. Here we report on the atomic and electronic structures triggered by ordered N vacancies in CrN films using modern TEM techniques combined with *ab initio* calculations.

II. METHODS

The CrN coatings used in this study were grown using a Cr interlayer on 300 and 500 μm thick Si(100) wafers by direct current unbalanced magnetron sputtering from a hot pressed Cr target (Ø 145 mm) in an industrial-scale Oerlikon Balzers rapid coating system (RCS) in static mode at a constant total pressure of 1 Pa. A target power of 6 kW and a temperature of 350 °C were used to deposit the films in a pure Ar atmosphere (Cr) and in an Ar + N_2 gas mixture with a nitrogen partial pressure of 0.25 Pa (CrN).

A TEM/STEM JEOL2100F operated at 200 kV and equipped with an image-side C_S corrector and an image filter (Tridiem) was used. The atomic resolution of this C_S-corrected microscope at 200 kV is better than 1.4 Å. The HRTEM images presented here were recorded on a $2k \times 4k$ pixel CCD camera at a magnification of 800 000 × or 1 500 000 × under a small C_S value of 7.0 μm. A STEM-EELS spectrum image was acquired using a dispersion of 0.2 eV/channel, a collection semiangle of 10 mrad, and a convergence semiangle of 7.5 mrad. The minimum achievable probe is about 0.2 nm in diameter, and the acquisition time was set to 1.0 s for core-loss spectrum and 0.001 s for low-loss spectrum. Multivariate statistical analysis was applied to the raw data of the spectrum images.[25] EELS quantification was performed using the Hartree-Slater model under a signal window of 60 eV for Cr-$L_{2,3}$ and of 80 eV for N-K edges, respectively. To determine the white-line ratio (L_3/L_2 ratio), the net signal of Cr-L_3 and Cr-L_2 needs to be acquired. First, the background for each spectrum was removed using a power-law function, and the Hartree-Slater models were used to fit the L_2 and L_3 edges. The theoretical cross sections were subtracted within the signal window of 569.4–577.4 eV for Cr-L_3 and of 578–586 eV Cr-L_2, respectively, in order to obtain a net intensity for respective L_2 and L_3 edges.

All the *ab initio* calculations are carried out within the framework of a total-energy plane wave density-functional theory pseudopotential approach, as implemented in the Vienna *ab initio* simulation package (VASP).[26] The Perdew-Burke-Ernzerhof exchange-correlation functional[27] is used in the Hamiltonians for solving the Kohn-Sham equations. Bulk CrN has a face centered cubic structure of NaCl ($B1$) prototype, which possesses a rhombohedral primitive cell with one Cr atom sitting at (0, 0, 0) coordinate and one N atom sitting at (1/2,1/2,1/2) coordinate. A 2 × 2 × 2 extended unit cell containing 16 atoms is generated for the perfect lattice structure (Fig. 1), and an 11 × 11 × 11 Monkhorst-Pack[28] mesh is used for the Brillouin-zone sampling. Defective structures are created by removing one, two, and four N atoms in this unit cell for vacancy concentrations of 6.25% (the corresponding atomic ratio of N/Cr = 0.875, Cr8N7), 12.5% (N/Cr = 0.75, Cr8N6), and 25 at.% (N/Cr = 0.5, Cr8N4), respectively. The equilibrium lattice constant is obtained by varying the cell volume, and fitting the energy-volume curve by the SJEOS method.[29] For a pure CrN structure, the calculation without spin polarization gives an equilibrium lattice constant of 4.05 Å. It is ∼3% lower than the experimental value (4.14 Å).[30] The difference is small and can be attributed to the influences from structure and antiferromagnetic coupling.[31] N vacancies are introduced in the cell for the defective structures. For one vacancy, that is, $c = 6.25$ at.%, all N lattice sites are equivalent, see the labeled positions in Fig. 1. But for more than one vacancy there are several possible combinations of lattice sites. For this reason we vary the vacancy sites for higher vacancy concentrations. At $c = 12.5$ at.% we delete N atoms 1 and 6 for one configuration, and N atoms 3 and 6 for another configuration. The lattice constant obtained from these two configurations is 3.977 Å with negligible difference. At $c = 25$ at.% we delete N atoms 1, 3, 6, and 8 for one configuration, and N atoms 2, 4, 5, and 7 for another configuration. For both cases lattice constants of 3.887 Å are obtained. The ratio of the lattice constant, defined as $(\frac{a(c)}{a(o)})_{\text{cal}}$, is plotted as a function of vacancy concentration c, where $a(c)$ and $a(0)$ are the lattice constants of defective and defect-free structures.

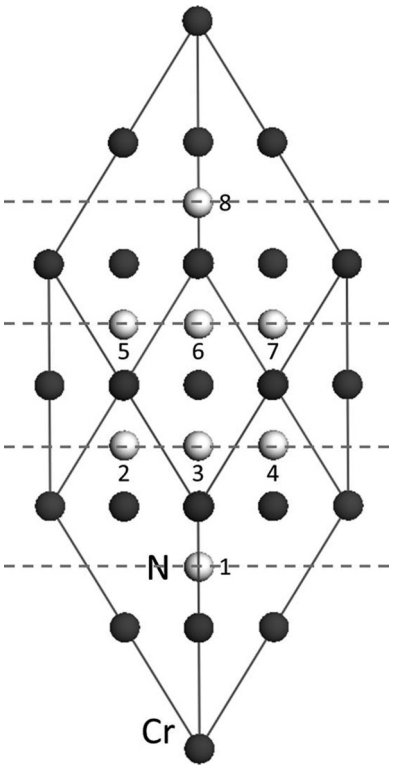

FIG. 1. The 2 × 2 × 2 extended rhombohedral cell for bulk CrN. Cr and N atoms are represented by dark and white circles, respectively. N atoms are labeled from 1 to 8 in four (111) planes drawn with dashed lines.

III. RESULTS AND DISCUSSIONS

A. HRTEM

1. Imaging along [110] and [100]

Independent of the substrates used, the CrN films grow frequently in a fine grained randomly oriented microstructure at the initial stage and then continuously grow at a columnar manner. However, when a Cr interlayer is introduced in between CrN and substrate, CrN can grow directly on the Cr layer.[32] The columnar grain is about 60–100 nm in width. To examine the atomic and electronic structure of the interface in more detail, a big columnar grain is selected for the atomic resolved imaging.

A C_S-corrected HRTEM image [Fig. 2(a)] acquired in the [110] direction shows some "stripe" features along the {111} plane adjacent to the Cr/CrN interface, forming a "defective layer" (CrN_x) in the film. The thickness of the defect layer is in the range of a few to tens of nanometers. Individual diffractograms shown in Fig. 2(b) (obtained by fast Fourier transform (FFT) based on the HRTEM image in the different regions in Fig. 2(a) illustrate that the defective layer possesses the identical pattern as the bulk CrN except a slight expansion, which means that it retains the same crystal structure

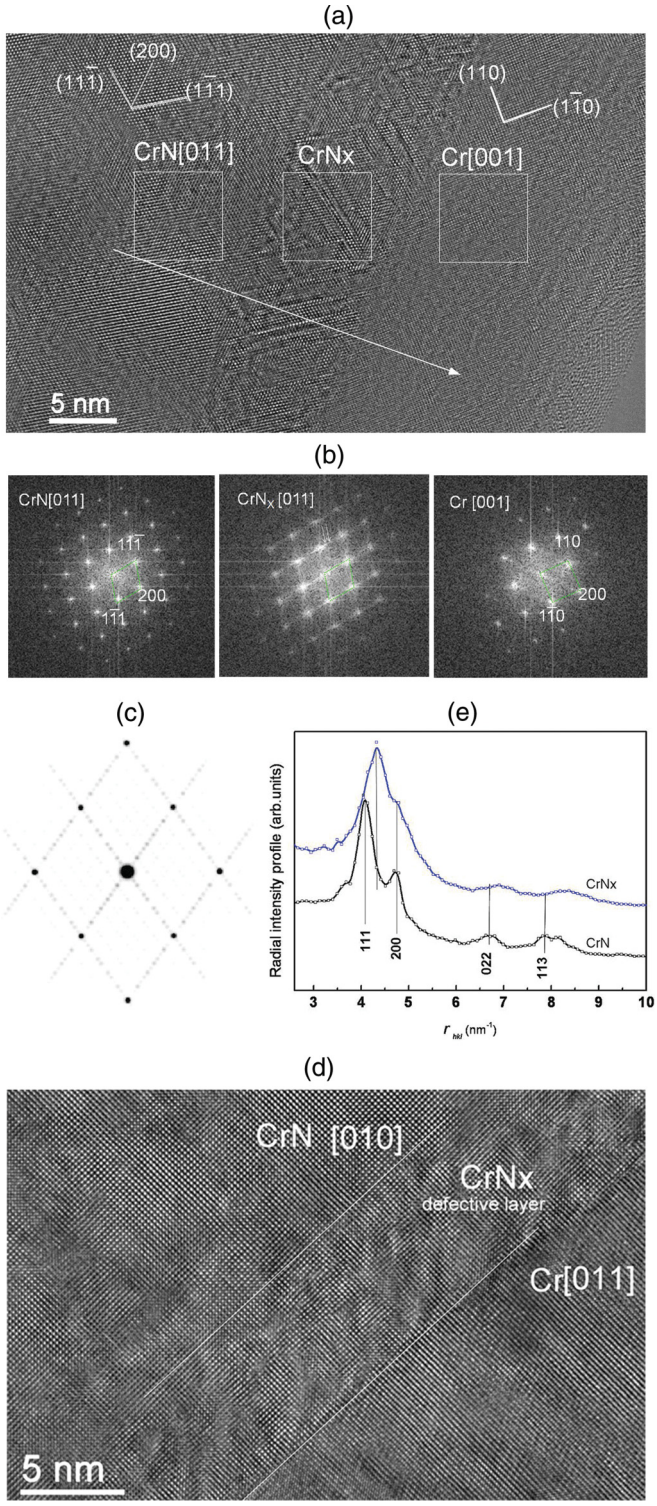

FIG. 2. (Color online) (a) A typical C_S-corrected HRTEM image of the CrN/Cr interface recorded along CrN [011] direction. A "defective" layer in between Cr and CrN exhibits apparent "stripe" features resulting from the ordered N vacancies well distributed at the {111} planes. (b) Individual diffractograms taken from a square area (labeled) in each layer. The crystallographic orientation relationships are Cr [001] ‖CrN [011] and Cr (100)‖ CrN (100). The diffractograms from the defective layer and nearby perfect CrN are almost identical due to the same structure (as labeled by the rhombus in the pattern). Note that the spots in the diffractogram acquired from the defective layer are relatively dispersed as compared to the nearby "perfect" CrN, and tiny spots as indicated by arrows. (c) A calculated diffraction pattern based on a supercell with a certain amount of N atoms in {111} planes intentionally removed, which set proof that the tiny spots along the {111} most likely originate from the ordered N vacancies. (d) A typical C_S-corrected HRTEM image recorded along the CrN [001] direction, where the defective layer approximately designated by two white lines near the interface appears as many strongly distorted regions relative to the nearby bulk. (e) The radial intensity distributions obtained from the FFTs of the defective and perfect region in the HRTEM image. Note that a line along which the EELS line scan was performed is schematically shown in (a).

as the CrN, of *fcc* lattice [which is also corroborated by the HRTEM image from the [010] direction, Fig. 2(d)], but possess a slight different lattice constant. It should be noted that this is different from the case that a new *hex* Cr2N phase forms,[13] thus showing a dissimilar diffractogram. The electron diffraction calculations, which intentionally introduced some ordered N vacancies along the {111} planes in a CrN supercell, largely reproduced the identical features, that is, satellite spots between two {111} spots as shown in Fig. 2(c). This means that when the N vacancies are well ordered and distributed in the {111} plane it can generate many tiny reflections between two {111} spots, presenting similar features as the observed diffractogram [Fig. 2(b)] shows. This provides direct evidence to prove the ordered N vacancy distributions. Moreover, the polycrystalline ring pattern calculations reveal that ordered N vacancies can lead to changes of intensity ratios of {111} and {200} reflections.[33] Detailed EELS analysis given in the following section evidently shows the N deficiencies in the defective layer. Taken together, it turns out that the stripe features experimentally observed originates from a large amount of N atoms missing at the {111} planes, resulting in the formation of numerous ordered N vacancies in the films. This is accompanied with stacking faults appearing at the {111} planes and considerable distortions in the films.

As the preceding analysis reveals, the stripe features result from the ordered N vacancies distribution (as also confirmed later by detailed analysis of diffractogram and EELS). However, the ordered N vacancies become not visible when viewed from the [100] direction. Instead, they show up as more strongly distorted regions in contrast to the "perfect" nearby bulk regions as shown in Fig. 2(d). The strong distortions in the film give an inhomogeneous contrast over a large area at the interface region. The deficiency of N atoms in CrN leads to a distorted lattice and a reduced lattice constant. According to the HRTEM image of CrN [011] [Fig. 2(a)], the intensity profiles acquired by radially averaging the intensity of spots in the diffractogram [Fig. 2(e)], similar to a Debye-Scherrer ring, were applied to visualize the tiny variation of interplanar spacings in CrN_x and CrN. The peaks in the profile correspond to the spot in Fig. 2(b). The comparison shows that the peaks slightly shift due to the presence of the ordered N vacancy. Based on the peak shift in the profile, using quantitative measurements we can evaluate the lattice constant variation in this region. A slight reduction of lattice constant in the defective CrN is found and determined after carefully calibrating the image (using

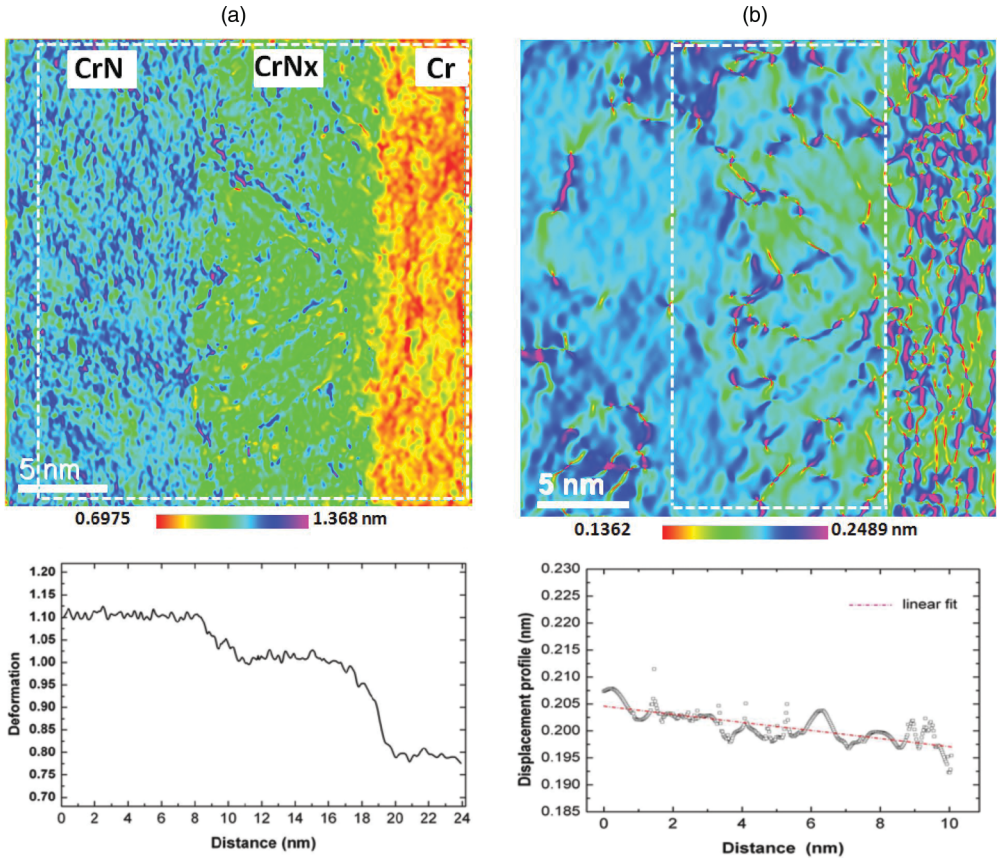

FIG. 3. (Color online) (a) The distortion map obtained using the reflections from the Cr layer [see Fig. 2(b)] clearly showing three distinct regions, a line profile crossing three layers integrated from a rectangular region from top to bottom attached below. (b) The $d_{(200)}$ displacement map acquired using the CrN (200) reflection, and an integrated line profile over a distance of ~12 nm as labeled by a rectangular region, starting at CrN about 3.0 nm away from CrN/CrN$_x$ interface and ending at the CrN$_x$/Cr interface is shown below. The linear fit curve is labeled in red.

the Cr layer and Si substrate as a internal standard). A high-precision measurement performed on the defective CrN over a certain area as indicated gives a value of 3.91 Å using 111, or 4.08 Å using 200. It is smaller than the lattice constant acquired in the perfect area (defect-free area), that is, 4.16 Å, which is almost identical to the equilibrium lattice constant given in the literature (i.e., 4.14 Å).[30] A difference in the lattice constant of $\Delta a = 0.25$ Å or $\Delta a = 0.06$ Å is obtained, which obviously results from the presence of the ordered N vacancies in the defect layer. According to the measured lattice constant, the N vacancy concentration contained in the film can be known if a relationship between the N vacancy concentration and a reduction of lattice constant is established beforehand. Similarly to the calculations, here, the experimentally determined ratio of lattice constant $(\frac{a(c)}{a(o)})_{\text{exp}}$ is expressed, where $a(c)$ and $a(0)$ are the lattice constant acquired from the defective layer and nearly defect-free bulk region, respectively.

2. *Distortion analysis*

Apart from the above distortion analysis implemented over a certain area in the layers, the strong distortions at an individual location can also be visualized using the geometrical phase analysis.[34,35] The distortion mapping performed at the same region [in Fig. 2(a)] clearly shows three distinguishable regions [Fig. 3(a)]. The corresponding integrated line profile crossing the three layers shows a different magnitude of distortions. Evidently, relative to the prefect CrN layer, the defective layer is slightly compressed while it is somewhat expanded referring to the Cr layer. The distortion distributions in the defective layer appears inhomogeneous, which may imply the presence of anisotropic distortion distributions attributed to the nitrogen vacancy located at the {111} planes.

The displacement map (d_{200}) performed on the same region is acquired using the CrN (200) reflection as shown in Fig. 3(b). As the defective layer retains the cubic structure and assuming a direct relationship between the structure and composition, the displacement map actually demonstrates the lattice constant ($2 \times d_{200}$) variations with the N vacancy, which gives displacement information at each individual position as comparing with the analysis of the "Debye-Scherrer ring." An integrated line profile spanning from the perfect CrN layer to the interface of CrN$_x$/Cr about 12 nm in length, which corresponds to the same distance as the EELS line scan carried out (within the range the N/Cr atomic ratio significantly changes), exhibits a distribution of the lattice constant. The strong fluctuations in the profile originate from the displacement singularities due to the presence of the defects. However, a linear relationship still can be found by fit, which is $d_{200} = (0.2067 - 7.6736 \times 10^{-4} \times d)$ nm, where d represents the distance. This also reflects the change of

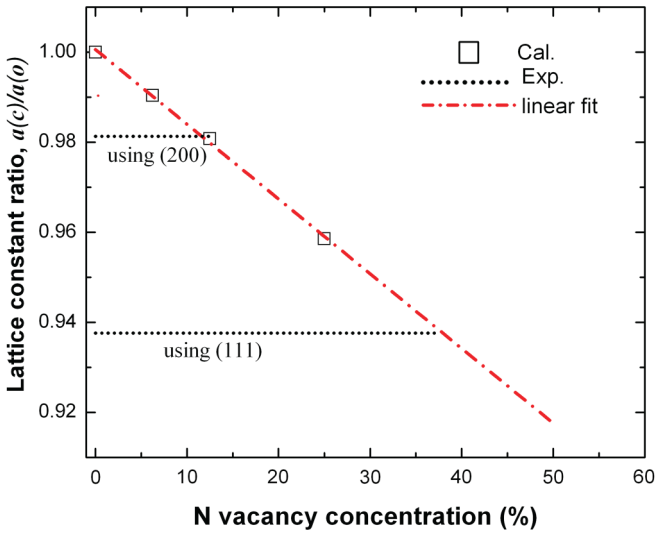

FIG. 4. (Color online) The calculated lattice constant ratio $[a(c)/a(0)]$ and the experimental measured lattice constant ratio obtained using (111) and (200) reflections plotted as a function of vacancy concentration, for the nonstoichiometric CrN_x the vacancy concentration is expressed as the $(1-x)/2 \times 100\%$ (N vacancy number divided by total atom number in CrN). The fit curve is labeled in red.

the lattice constant ($2 \times d_{200}$) within the measured distances, signifying that the lattice constant and N vacancy variations are closely relevant.

B. *Ab initio* calculations of the lattice constant

To explore the effect of N vacancy on the lattice constant of CrN, *ab initio* calculations were performed. Figure 1 is a $2 \times 2 \times 2$ extended rhombohedral cell for bulk CrN, where Cr and N atoms are represented by dark and white circles, respectively. N atoms are labeled from 1 to 8 in four {111} planes drawn with dashed lines. The effect of N vacancies on the lattice is closely investigated by relaxing the structure after removing the N atom sites in CrN. The calculated results are illustrated in Fig. 4. The ratio of lattice constant is plotted as a function of vacancy concentrations. A relationship between the N vacancy concentration and the reduction of the lattice constant is calculated, and is also shown (in red). From the plot, it is clearly seen that the higher the N vacancy concentration in the film, the smaller the ratio of lattice constant becomes. By means of the calculated relationship, N vacancy concentrations in the films can be reasonably derived. We insert the values obtained from experimental quantitative measurements into the plot using the (200) and (111) reflections recorded at a square region [in Fig. 2(a)] as indicated by a dotted line in Fig. 4. It is clearly seen that a corresponding vacancy concentration, ~12% or ~37%, in the region can be derived. As the N vacancy concentration is significantly distributed in the {111} planes, the derived vacancy concentration using (111) reflection is higher than that using (200). In terms of the relationship of lattice constant variation and N vacancy concentration, it is thus possible to evaluate the N vacancy concentration at each location by measuring the reduction of lattice constant using a C_S-corrected HRTEM image. However, it should be noted that in the present approach we assume that the nearby bulk CrN is stoichiometric. In fact, the stoichiometric CrN may contain randomly distributed individual vacancies, which might not be sensitive enough to be detected in the HRTEM image.

C. Electronic structures of nitrogen vacancy

Numerous N vacancies can induce changes of the electronic structure of the CrN films. STEM-EELS analysis was performed along the line labeled in Fig. 2 (for brevity, only five spots are shown, and the corresponding N/Cr ratios are indicated) across the interface regions. The relative atomic concentration distribution across the interface region was determined using EELS elemental quantifications [Fig. 5(a)]. Three distinct regions can be seen when scanning from CrN to Cr. A substoichiometric layer with a variable ratio of Cr to N evidently exists between CrN and pure Cr, which corresponds to a defective layer as shown in the HRTEM image [Fig. 2(a)]. The analysis indicates that the defective layer contains numerous N vacancies. The stripe features in the HRTEM image are essentially stacking faults due to the presence of the ordered nitrogen vacancies at the {111} planes. It should be mentioned that within a transition region of ~12 nm in width, the N vacancy concentration is different at each position probed by EELS, ranging from nearly 0 (CrN) to 100% (Cr). However, the N vacancy concentration deduced from the HRTEM images is averaged over a square area of about 10×10 nm^2 in the defective layer.

Low-loss and core-loss spectra from CrN, crossing the defective layer, to Cr show very small differences. Low-loss spectra of CrN [Fig. 5(b)] exhibit a small peak at around 12 eV, while it becomes reduced at the N vacancy rich layers and the Cr layer, however, presents as a shoulder and much overlap with the plasmon. It also clearly indicates that with increasing N vacancy concentration the volume plasmon peak slightly shifts to a lower energy position by a few eV and finally approaches the value of pure Cr.

The energy-loss near edge structure (ELNES) changes of Cr and N peaks recorded from the N vacancy rich region give more insights into the effect of N vacancy on the electronic structure of CrN. A small different characteristic is further demonstrated in the fine structures of Cr-$L_{2,3}$ in Cr, CrN as well as the defect layer [Fig. 5(c)]. The Cr-$L_{2,3}$ edge in the defective CrN layer shows a chemical shift as compared to Cr and stoichiometric CrN. Moreover, the comparison further indicates that the height of the L_2 peak clearly increases with decreasing N vacancy concentration. The minor onset difference in the L_3 edge clearly manifests a chemical shift to a low energy position with increasing N vacancy content. A detailed analysis on the ratio of the L_3/L_2 of Cr is shown in the next paragraph. Ordered N vacancies also modify the ELNES of the N-K edge [Fig. 5(d)]. In particular, the second peak at the corresponding N-K edge broadens and also decreases in the intensity, similar to the changes detected in VN_x.[22] The N-K edge significantly shifts to a higher energy position when the N vacancy concentration increases. Our experimental observation on the fine structure variations of the N-K edge shows a good agreement with the DFT calculations, where the N-K edge in the TiN and VN films is found to obviously

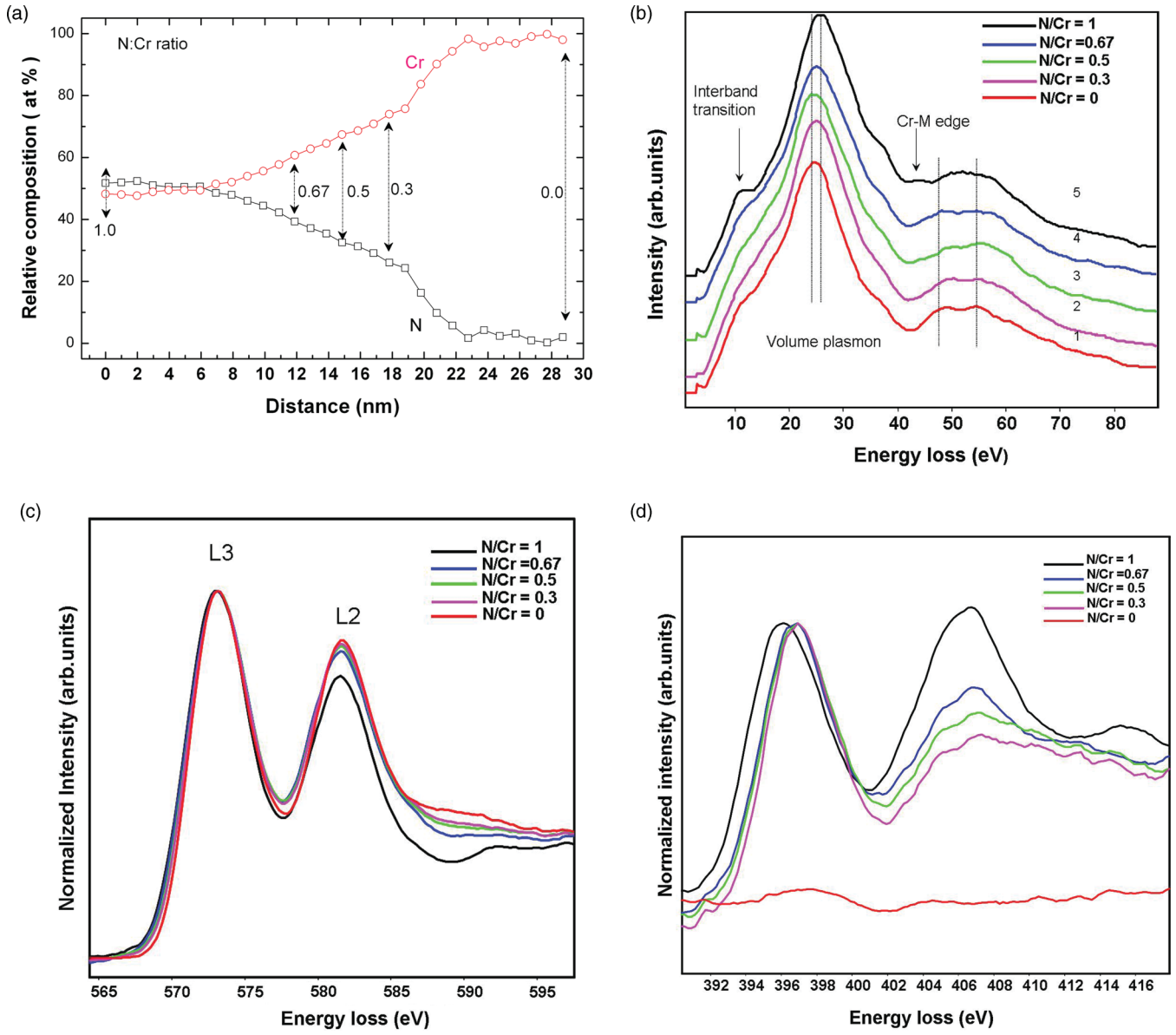

FIG. 5. (Color online) (a) Atomic concentration variations versus the probe position across the interface along the line schematically labeled in Fig. 2(a), in which only five selected spots are denoted with a ratio value. (b) The low-loss and core-loss spectra acquired from different locations. (c) The ELNES spectra of the Cr-$L_{2,3}$ edges normalized and aligned by using the L_3 edge for direct comparison showing that the increase of N vacancy concentrations not only changes the onset of spectra, but also the intensity of the L_2 edge. (d) The fine structures of the N-K edge showing that the first peak shifts to a higher energy position with increasing the N vacancy concentrations while the second peak is reduced in the intensity and finally disappears.

shift to a high energy position when numerous N vacancies are introduced.[23,36] It should be mentioned that the features observed in Cr-L and N-K in the defective CrN layer resembles those observed in the pure Cr_2N phase,[13] which actually corresponds to the case of the N/Cr atomic ratio = 0.5 in the present study. In contrast, in the present study, the effect of continuous N vacancy concentration change on the ELNES of Cr-L and N-K is clarified in detail and a generalized conclusion is drawn. Moreover, as discussed below, the iconicity change triggered by N vacancy is further unveiled.

L absorption edges in transition metals originate from the transition of electrons from the p state to unoccupied states above the Fermi level. L_3 and L_2 correspond to the transitions $2p1/2 \rightarrow 3d$ or $2p3/2 \rightarrow 3d$ states, respectively. The quantification for the $L_{2,3}$ intensity, that is, L_3/L_2 ratio, and energy positions, can offer insights into the electronic structure information about the valence state, spin and momentum, etc.[37,38] The L_3/L_2 ratios for Cr are sensitive to the electronic configuration or cation charge and can thus be used as a way of measuring charge state in microanalytical applications. This effect can therefore be used to measure the ionicity in EELS microanalysis of various materials.

Figure 6(a) illustrates the change of the L_3/L_2 ratio, together with the N/Cr ratio, as the incident probe moves from the stoichiometric CrN layer, to the substoichiometric layer with a higher concentration of N vacancy (defective

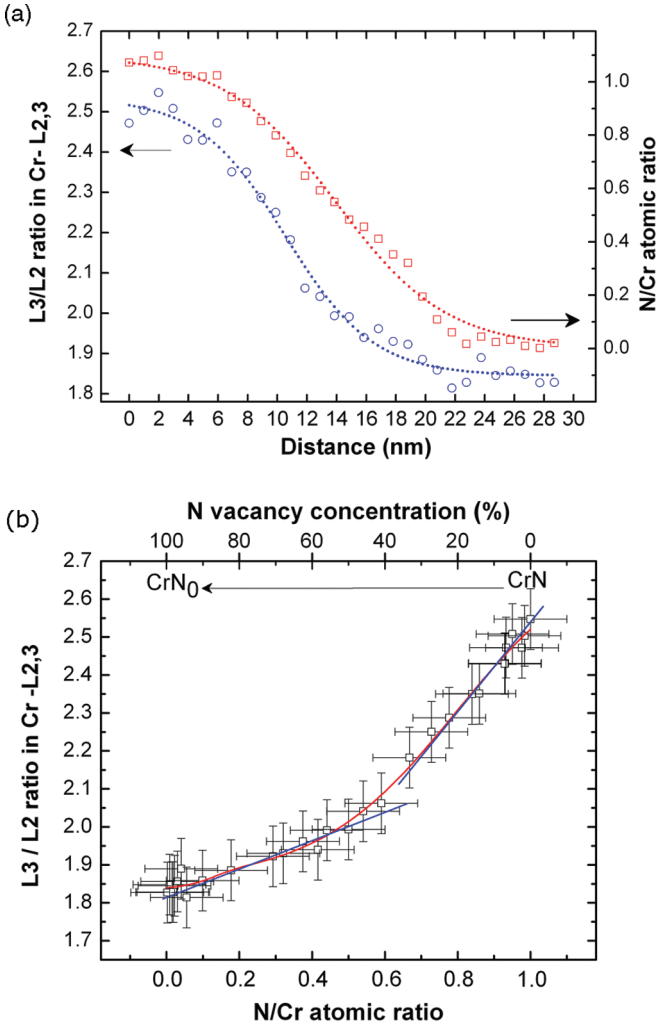

FIG. 6. (Color online) (a) The L_3/L_2 ratio and the N/Cr atomic ratio plotted as a function of probe position across the interface. The fit curves (dotted lines) for both reveal a similar tendency. (b) The variation of L_3/L_2 ratio expressed as a function of the N/Cr ratio or N vacancy concentration (red curve). Two different regimes indicated by blue lines are visible, which implies the presence of a critical N vacancy concentration.

layer), and to the Cr layer. Both show a very similar trend. A gradual decrease of the L_3/L_2 ratio is observed with decreasing the N/Cr ratio. Approaching the stoichiometric CrN or the metallic Cr, the L_3/L_2 ratio converges a different constant value, whereas it varies sensibly in between. This indicates that the $L_{2,3}$ ratio is closely linked to the N content. It can be understood that the N vacancies govern the charge redistributions. As a consequence the shape of the $L_{2,3}$ edge and the L_3/L_2 ratio change. In general, the higher the N vacancy content of the film, the more metallic the character of the film becomes. The plot shown in Fig. 6(a) reveals that a more metallic tendency in the defective CrN layer (substoichiometric layer) may exist as compared to the stoichiometric CrN film. The same conclusion can be drawn from a close comparison of the ELNES of the Cr-L edge, from stoichiometric CrN to substoichiometric CrN_x, and to metallic Cr, the L_2 edge becomes more narrow and sharp, and is accompanied by a relative chemical shift.

According to the Fig. 6(a), a linear relationship between the L_3/L_2 and the N/Cr ratio (or N vacancy concentration) can be further established [Fig. 6(b)], where a clear correlation is found. It is noted that the L_3/L_2 ratio nonlinearly changes (as the fitted curve indicates), and within the error roughly presents two regimes with different slope when the N/Cr content varies from 0 to 1 (or N vacancy from 100% to 0). In general, the higher the N concentration (or the lower the N vacancy concentration) is, the higher the L_3/L_2 ratio. From the variation of the L_3/L_2 ratio, it is seen that close to 10% N vacancy concentration (or N/Cr $\geqslant$ 0.9) introduced into CrN_x it hardly changes, which means that CrN_x still preserves its ionic character. For more than 70% N vacancy concentration (N/Cr $\leqslant$ 0.3) in the CrN_x layer, the L_3/L_2 ratio approaches the value of Cr, indicating the apparent metallic character in the CrN_x. Interestingly, a turning point at a ratio of $\sim$0.55 (the ratio approximately corresponds to the composition of a Cr_2N phase) appears. Below this value the slope of the L_3/L_2 ratio becomes smaller, and seems to depend less on the N/Cr ratio. It can be reasonably inferred that the Cr charge states are different in the two regions and most likely the Cr ionicity has changed starting from stoichiometric CrN to CrN_x with a large amount of N vacancies brought in. Above $\sim$0.55, towards the stoichiometric CrN, the ionicity increases, whereas below the value, towards the Cr_2N, it exhibits a more covalent state, and towards the metallic Cr it shows more metallic character. It was actually reported that Cr_2N shows a strong covalent bonding.[39] Based on the careful measurement, we are able to determine the ionicity of CrN by means of the L_3/L_2 or the N/Cr ratio. It quantitatively reveals to which extent the N vacancy concentration can affect the ionicity in the CrN. It predicts that a continuous N vacancy variation leads to a transition from an ionic crystal to a covalent crystal and eventually approaches the metallic crystal, i.e., pure Cr. This means a vacancy driven transition from an insulator, to a semiconductor, and finally to a metallic conductor may occur in CrN_x. In summary, the relevant effect of composition, that is, N vacancy content, can be expressed in terms of the L_3/L_2 ratio or covalent-ionic level of the bonding. A critical N vacancy concentration most likely exists, which discriminates the ionic and covalent bonds in the CrN crystal. The mechanism behind this can be simply addressed as follows. With increasing N vacancy concentration, Cr-Cr atoms become close, and Cr-Cr distance somehow gets smaller. Local lattice relaxations and rearrangements of interatomic bonds thus take place, resulting in the appearance of strong Cr-Cr bonds and a reduction in the lattice parameter. To the end, the metallic level of the bonding dramatically increases when the N vacancy concentration exceeds a certain amount in CrN_x.

D. Relationship between the lattice constant and vacancy concentration

With the available data from the HRTEM image and EELS analysis performed at the same region crossing the defective layer, a generalized relationship between the lattice constant and N vacancy concentrations (or the N/Cr atomic ratio) can be further established. Using the fitted relationship of the lattice constant and distance [Fig. 3(b)], combined with the EELS data [Fig. 5(a)] acquired at the identical

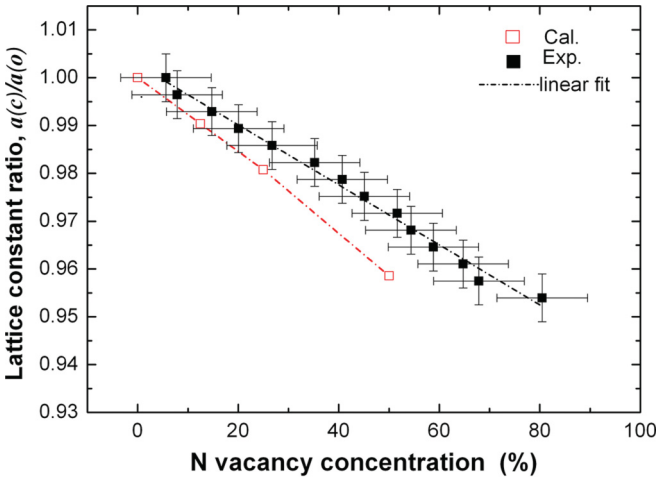

FIG. 7. (Color online) The relationship between the lattice constant ratio and N vacancy concentration. The open symbols are calculated using DFT, and dashed dotted lines are fitted by a linear function. Note that the N vacancy concentration is expressed as $(1-x)\times 100\%$ for the nonstoichiometric CrN_x in order to directly link with the N/Cr atomic ratio obtained by EELS. The error bar corresponds to 1% (10%) variation in the magnitude of the lattice constant ratio (N/Cr atomic ratio) in the defect-free region.

region, the variation of the lattice constant with the N vacancy concentration can be experimentally derived and plotted (Fig. 7). For comparison, the calculated relationship (in red) by DFT is inserted, where, for convenience, N vacancy concentration is expressed as $(1-x)\times 100\%$ for CrN_x, and the lattice constant is described as a lattice constant ratio. Very interestingly, it reveals that the experimentally measured and theoretically calculated relationships follow a similar tendency, and both display that the lattice constant gradually decreases with increasing the N concentration (or decreasing the N/Cr atomic ratio). It is seen that within the error it reaches a reasonable agreement. In fact, this uncovers a general relationship between the lattice constant and its composition in CrN (i.e., N vacancy effect). However, it should be pointed out that the structure transformation may occur when the N vacancy concentration exceeds a certain amount, which implies that the linear relationship between the lattice constant and vacancy concentration becomes invalidated.

E. Concluding remarks

To summarize, in this work we have used simultaneous imaging and spectroscopy to visualize the N vacancies in CrN. It is found that the ordered N vacancies are well distributed on {111} planes. Structurally, the ordered N vacancies lead to a significant lattice distortion and a reduction of the lattice constant. By means of the theoretical calculations, a relationship between the N vacancy concentration and the lattice constant is established, and the experimentally determined N vacancy concentration is possible. The ordered N vacancies further induce the electronic changes of CrN. Detailed analysis shows that the white-line ratio, the N vacancy concentrations and the covalent-ionic level of the bonding are intrinsically relevant. The relationship between the ionicity in CrN and nitrogen vacancy concentration is revealed. Furthermore, the comparison of experimentally measured and theoretically calculated relationship between the lattice constant and N vacancy concentration gives a reasonable agreement.

ACKNOWLEDGMENTS

Gabriele Moser and Herwig Felber are gratefully acknowledged for their help with the sample preparation.

[1] L. Hultman, Vacuum **57**, 1 (2000).
[2] G. Berg, C. Friedrich, E. Broszeit, and C. Berger, Surf. Coat. Technol. **86-87**, 184 (1996).
[3] C. Rebholz, H. Ziegele, A. Leyland, and A. Matthews, Surf. Coat. Technol. **115**, 222 (1999).
[4] L. M. Corliss, N. Elliott, and J. M. Hastings, Phys. Rev. **117**, 929 (1960).
[5] D. Gall, C. S. Shin, R. T. Haasch, I. Petrov, and J. E. Greene, J. Appl. Phys. **91**, 5882 (2002).
[6] K. Inumaru, K. Koyama, N. Imo-oka, and S. Yamanaka, Phys. Rev. B **75**, 054416 (2007).
[7] A. Herwadkar and W. R. L. Lambrecht, Phys. Rev. B **79**, 035125 (2009).
[8] X. Y. Zhang and D. Gall, Phys. Rev. B **82**, 045116 (2010).
[9] R. Daniel, K. J. Martinschitz, J. Keckes, and C. Mitterer, Acta Mater. **58**, 2621 (2010).
[10] P. A. Bhobe, A. Chainani, M. Taguchi, T. Takeuchi, R. Eguchi, M. Matsunami, K. Ishizaka, Y. Takata, M. Oura, Y. Senba, H. Ohashi, Y. Nishino, M. Yabashi, K. Tamasaku, T. Ishikawa, K. Takenaka, H. Takagi, and S. Shin, Phys. Rev. Lett. **104**, 236404 (2010).
[11] X. Y. Zhang, J. S. Chawla, B. M. Howe, and D. Gall, Phys. Rev. B **83**, 165205 (2011).
[12] X. Y. Zhang, J. S. Chawla, R. P. Deng, and D. Gall, Phys. Rev. B **84**, 073101 (2011).
[13] Z. L. Zhang, R. Daniel, and C. Mitterer, J. Appl. Phys. **110**, 043524 (2011).
[14] J. D. Browne, P. R. Liddell, R. Street, and T. Mills, Phys. Status Solidi A **1**, 715 (1970).
[15] C. Constantin, M. B. Haider, D. Ingram, and A. R. Smith, Appl. Phys. Lett. **85**, 6371 (2004).
[16] M. Guemmaz, A. Mosser, and J.-C. Parlebas, J. Electron Spectrosc. Relat. Phenom. **107**, 91 (2000).
[17] S.-H. Jhi, S. G. Louie, M. L. Cohen, and J. Ihm, Phys. Rev. Lett. **86**, 3348 (2001).
[18] R. Sanjinés, C. Wiemer, P. Hones, and F. Lévy, J. Appl. Phys. **83**, 1396 (1998).
[19] L. Porte, L. Roux, and J. Hanus, Phys. Rev. B **28**, 3214 (1983).
[20] K. Suenaga, C. Colliex, C. Sant, S. Labdi, and P. Houdy, J. Phys. Soc. Jpn. **66**, 2097 (1997).
[21] S. Terada, K. Asayama, M. Tsujimoto, H. Kurata, and S. Isoda, Microsc. Microanal. **15**, 106 (2009).

[22]F. Hofer, P. Warbichler, A. Scott, R. Brydson, I. Galesic, and B. Kolbesen, J. Microsc. **204**, 166 (2001).
[23]P. Lazar. J. Redinger, J. Strobl, R. Podloucky, B. Rashkova, G. Dehm, G. Kothleitner, S. Šturm, K. Kutschej, C. Mitterer, and C. Scheu, Anal. Bioanal. Chem. **390**, 1447 (2008).
[24]L. Tsetseris, N. Kalfagiannis, S. Logothetidis, and S. T. Pantelides, Phys. Rev. Lett. **99**, 125503 (2007).
[25]M. Bosman, M. Watanabe, D. T. L. Alexander, and V. J. Keast, Ultramicroscopy **106**, 1024 (2006).
[26]G. Kresse and J. Furthmuller, Phys. Rev. B **54**, 11169 (1996).
[27]J. P. Perdew, K. Burke, and M. Ernzerhof, Phys. Rev. Lett. **77**, 3865 (1970).
[28]H. J. Monkhorst and J. D. Pack, Phys. Rev. B **13**, 5188 (1976).
[29]A. B. Alchagirov, J. P. Perdew, J. C. Boettger, R. C. Albers, and C. Fiolhais, Phys. Rev. B **63**, 224115 (2001).
[30]P. Villars and L. D. Calvert, *Pearson's Handbook of Crystallographic Data for Intermetallic Phases* (American Society for Metals, Metals Park, OH, 1986).
[31]M. S. Miao and W. R. L. Lambrecht, Phys. Rev. B **71**, 214405 (2005).
[32]S. Han, H.-Y. Chen, Z.-C. Chang, J.-H. Lin, C.-J. Yang, F.-H. Lu, F.-S. Shieu, and H. C. Shih, Thin Solid Films **436**, 238 (2003).
[33]X. Z. Li, J. Zhang, and D. J. Sellmyer, J. Appl. Cryst. **37**, 1010 (2004).
[34]A. K. Gutakovskii, A. L. Chuvilin, and S. A. Song, B. Russ. Acad: Phys. **71**, 1426 (2007).
[35]M. J. Hytch, E. Snoeck, and R. Kilaas, Ultramicroscopy **74**, 131 (1998).
[36]M. Tsujimoto, H. Kurata, T. Nemoto, S. Isoda, S. Terada, and K. Kaji, J. Electron Spectros. **143**, 159 (2005).
[37]W. G. Waddington, P. Rez, I. P. Grant, and C. J. Humphreys, Phys. Rev. B **34**, 1467 (1986).
[38]R. D. Leapman, L. A. Grunes, and P. L. Fejesf, Phys. Rev. B **26**, 614 (1982).
[39]R. Sanjinés, P. Hones, and F. Lévy, Thin Solid Films **332**, 225 (1998).